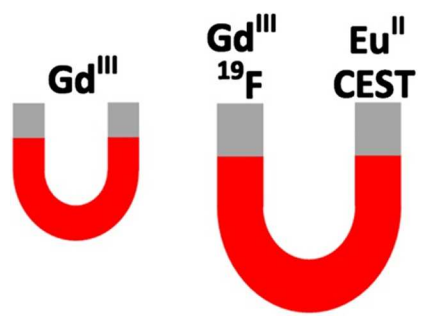




## Enhancing Magnetic Resonance Imaging with Contrast Agents for Ultra-High Field Strengths

|                               |   |
|-------------------------------|---|
| Journal:                      | <i>Analyst</i>  |
| Manuscript ID:                | AN-MRV-05-2014-000990.R1  |
| Article Type:                 | Minireview  |
| Date Submitted by the Author: | 20-Jun-2014   |
| Complete List of Authors:     | Kuda-Wedagedara, Akhila; Wayne State University, Chemistry<br>Allen, Matthew; Wayne State University, Chemistry |
|                               |   |

1  
2  
3  
4  
5  
6  
7  
8  
9  
10  
11  
12  
13  
14  
15  
16  
17  
18  
19  
20  
21  
22  
23  
24  
25  
26  
27  
28  
29  
30  
31  
32  
33  
34  
35  
36  
37  
38  
39  
40  
41  
42  
43  
44  
45  
46  
47  
48  
49  
50  
51  
52  
53  
54  
55  
56  
57  
58  
59  
60



New strategies for contrast agents enable effective magnetic resonance imaging at ultra-high magnetic field strengths.

## MINIREVIEW

## Enhancing Magnetic Resonance Imaging with Contrast Agents for Ultra-High Field Strengths

/Cite this: DOI: 10.1039/x0xx00000x

Akhila N. W. Kuda-Wedagedara<sup>a</sup> and Matthew J. Allen<sup>a</sup>

Received 00th May 2014,

Accepted 00th May 2014

DOI: 10.1039/x0xx00000x

www.rsc.org/

Contrast agents are diagnostic tools that often complement magnetic resonance imaging. At ultra-high field strengths ( $\geq 7$  T), magnetic resonance imaging is capable of generating desirable high signal-to-noise ratios, but clinically available contrast agents are less effective at ultra-high field strengths relative to lower fields. This gap in effectiveness demands the development of contrast agents for ultra-high field strengths. In this minireview, we summarize contrast agents reported during the last three years that focused on ultra-high field strengths.

### Introduction

Magnetic resonance imaging (MRI) is a non-invasive technique that can map the relaxation rates of water protons in a magnetic field to generate images. Common clinical magnetic field strengths are 1.5 and 3 T, but the number of higher field strength systems increases each year. Over forty clinical and preclinical 7 T MRI scanners are available in the United States, and many higher field strength scanners ( $\geq 7$  T) are used in preclinical research.<sup>1–4</sup>

Magnetic fields at or above 7 T are classified as ultra-high field strengths, and the use of 7 T magnets for clinical MRI has been reported.<sup>5–8</sup> There is a strong urge to use ultra-high field MRI scanners because of the advantages that can be gained with ultra-high field strengths relative to lower field strengths, including high signal-to-noise ratios, high spatial resolution, short acquisition times, and the ability to use low sensitivity nuclei other than <sup>1</sup>H (including <sup>19</sup>F, <sup>13</sup>C, <sup>23</sup>Na, and <sup>31</sup>P).<sup>2–4</sup> These advantages are demonstrated by the increased amount of information that can be gained from MR images at ultra-high field strengths compared to lower field strengths (Fig. 1).

Obtaining high quality MR images (high contrast-to-noise ratios) is critical in diagnosing diseases, but increases in magnetic field strength alone are not always sufficient to obtain images with high contrast-to-noise ratios. High contrast-to-noise ratios often can be achieved using paramagnetic metal complexes called contrast agents.<sup>9</sup> For example, complexes 1–6 shown in Fig. 2 are clinically approved contrast agents that are used to improve contrast-to-noise ratios in MR images in approximately half of all clinical scans.<sup>9–12</sup> Contrast agents influence both longitudinal ( $1/T_1$ ) and transverse ( $1/T_2$ ) relaxation rates, and clinically approved contrast agents can be categorized into two types of agents: those with  $T_1/T_2$  ratios close to one ( $T_1$ -shortening or positive agents) and those with  $T_1/T_2$  ratios  $\geq 6$  ( $T_2$ -shortening or negative agents).<sup>12,13</sup> Both types of contrast agents usually contain paramagnetic metal ions that increase the relaxation rates ( $1/T_1$  and  $1/T_2$ ) of the protons of the surrounding molecules, but current clinical contrast agents are less effective at ultra-high magnetic fields than at lower fields (Table 1).<sup>14–16</sup> Note: care should be taken to only compare relaxivity values reported at the same temperature and in the same solvent.

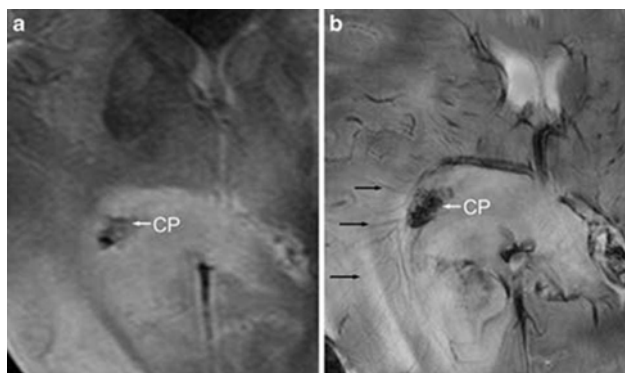


**Fig. 1** MR images of an axial slice of a human brain at (a) 1.5 and (b) 7 T. The image acquired at 7 T enables visualization of blood vessels (black arrows) and choroid plexus (CP, an abnormality in the right lobe) that are not clearly visible at 1.5 T.<sup>7</sup> Reprinted from C. Moeninghoff, S. Maderwald, J. M. Theyssohn, O. Kraff, M. E. Ladd, N. El Hindy, J. van de Nes, M. Forsting and I. Wanke, Imaging of Adult Astrocytic Brain Tumours with 7 T MRI: Preliminary Results, *Eur. Radiol.*, 2010, **20**, 704–713, with kind permission from Springer Science and Business Media.

Because of the decrease in relaxivity with increasing field strength, a great deal of research has focused on modifying Gd<sup>III</sup>-based agents to increase relaxivity at ultra-high field strengths. Additionally, other types of contrast agents have been studied to meet the need of efficient contrast agents at ultra-high fields. Much of this work has been reviewed,<sup>13,17–25</sup> and this review is intended to describe both Gd<sup>III</sup>-based and non-Gd<sup>III</sup>-based strategies to influence contrast in ultra-high field MRI from the last three years with a focus on discrete molecules. For reviews focused on nanoparticles, we suggest a few other reviews.<sup>26–31</sup> This review is divided into four sections: (1) optimization of Gd<sup>III</sup>-based agents;

## MINIREVIEW

(2) Eu<sup>II</sup>-containing cryptates as  $T_1$ -shortening agents; (3) <sup>19</sup>F-MRI agents; and (4) chemical exchange saturation transfer agents.

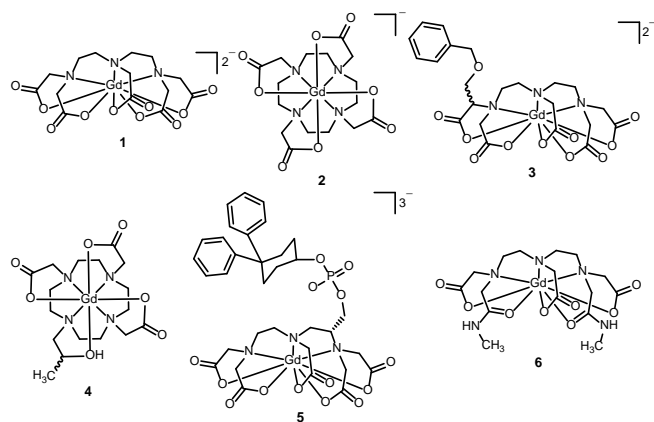


**Fig. 2** Clinically approved contrast agents: Gd<sup>III</sup>-containing diethylenetriaminepentaacetate (DTPA), **1**; Gd<sup>III</sup>-containing 1,4,7,10-tetraazacyclododecane-1,4,7,10-tetraacetate (DOTA), **2**; Gd<sup>III</sup>-containing  $\alpha$ -(benzyloxymethyl)diethylenetriaminepentaacetate (BOPTA), **3**; Gd<sup>III</sup>-DOTA derivative **4**; and Gd<sup>III</sup>-DTPA derivatives **5** and **6** (coordinated water molecules and counter ions are not shown for clarity).

**Table 1** Relaxivities ( $\text{mM}^{-1} \text{s}^{-1}$ ) per-Gd<sup>III</sup> of  $T_1$ -shortening contrast agents at 37 °C in blood.<sup>32,33</sup>

| Complex  | 1.5 T | 3 T  | 7 T |
|----------|-------|------|-----|
| <b>1</b> | 4.3   | 3.6  | 3.4 |
| <b>2</b> | 4.2   | 3.6  | 3.4 |
| <b>3</b> | 6.7   | 5.8  | 4.8 |
| <b>4</b> | 4.4   | 3.5  | 3.3 |
| <b>5</b> | 19    | 11.3 | 5.4 |
| <b>6</b> | 4.6   | 3.9  | 3.7 |

### (1) Optimization of Gd<sup>III</sup>-Based Agents

Molecular parameters that influence the relaxivity of  $T_1$ -shortening agents include the number of coordinated water molecules and the electronic relaxation, water-exchange, and rotational correlation rates. This review does not go into detail regarding these properties because they have been described elsewhere;<sup>34–37</sup> however, at field strengths higher than 1.5 T, the electronic relaxation rates do not contribute significantly to relaxivity,<sup>37</sup> but water-exchange and rotational correlation rates need to be optimized as a function of field strength to achieve fast longitudinal relaxation rates of the protons of the surrounding molecules.<sup>36</sup> Another parameter that influences relaxivity is the number of coordinated water molecules. Increasing this number usually increases relaxation rates but often leads to complexes with lowered kinetic stabilities.<sup>38</sup> However, incorporation of multiple complexes into one molecule is a way to influence the rotational correlation rate and the number of coordinated water molecules without necessarily sacrificing kinetic stability.

Apart from the number of coordinated water molecules, the relaxivities of clinically used  $T_1$ -shortening contrast agents (**1–6**, Fig. 2) are limited by fast rotational correlation rates (water-exchange rates do not play a large role in relaxivity at ultra-high fields for Gd<sup>III</sup>-based  $T_1$ -shortening agents until rotational correlation rates have been optimized);<sup>13</sup> therefore, optimizing rotational correlation rates is essential to achieve high relaxivity. To

slow rotational correlation rates, conjugation to relatively large molecules such as proteins has been studied (the use of macromolecules also influences biodistribution and half-life in vivo).<sup>39–41</sup> Although macromolecule-conjugation is effective at lower field strengths ( $\leq 3$  T), this strategy causes too much slowing of the rotational correlation rates and negatively impacts relaxivity at ultra-high field strengths. To achieve the best relaxivity above 3 T, it is necessary to bring the rotational correlation rate to an intermediate range ( $2.5 \times 10^8$  to  $2 \times 10^9 \text{ s}^{-1}$ ).<sup>36,38</sup> Rotational correlation rate is influenced by the molecular weight and flexibility of a complex; therefore, by slightly increasing the steric bulk or by linking multiple Gd<sup>III</sup>-containing complexes together, the rotational correlation rate can be targeted to the desired region for a specific field strength.<sup>13</sup>

Meade and co-workers reported the conjugation of multiple Gd<sup>III</sup>-containing complexes via 5-(2,4,6-triethenylphenoxy)pentanoic acid to produce trimeric complex **7** with rigid triazole linkers to bring the rotational correlation rate to an intermediate range (Fig. 3).<sup>42</sup> Complex **7** displays a 170% higher per-Gd relaxivity (Table 2) at ultra-high fields compared to unconjugated complex **8** due to the decrease in rotational correlation rate from  $2 \times 10^{10}$  to  $1.7 \times 10^9 \text{ s}^{-1}$ .<sup>42</sup>

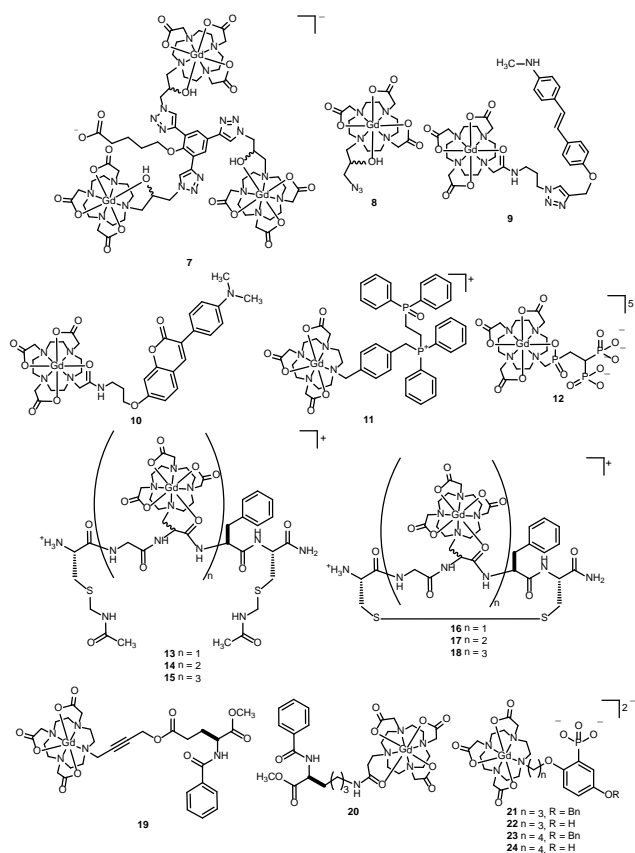


**Fig. 3** Chemical structures of contrast agents **7–24** (coordinated water molecules and counter ions are not shown for clarity).

Another example of optimizing rotational correlation rate was reported by Yang and co-workers.<sup>43</sup> They metalated the apo proteins ProCA1 and polyethylenglycol (PEG)-conjugated ProCA1 with Gd<sup>III</sup> (Fig. 4). The relaxivities of PEGylated Gd<sup>III</sup>-containing ProCA1 proteins are higher at ultra-high field strengths than non-PEGylated Gd<sup>III</sup>-containing ProCA1 (Fig. 4B) and Gd<sup>III</sup>-DTPA due to the slowing of rotational correlation rate and the increase in

water-coordination number (water-coordination numbers: Gd<sup>III</sup>-DTPA = 1.1, Gd<sup>III</sup>-containing ProCA1 = 2.4, and Gd<sup>III</sup>-containing PEGylated ProCA1 = 3.0).

**Table 2** Relaxivities (mM<sup>-1</sup> s<sup>-1</sup>) per-ion of T<sub>1</sub>-shortening contrast agents at 37 °C (unless otherwise noted) and 1.4, 3, 4.7, 7, 9.4, and 11.7 T.

| Complex | 1.4              | 3.0               | 4.7 | 7.0               | 9.4              | 11.7 | Reference |
|---------|------------------|-------------------|-----|-------------------|------------------|------|-----------|
| 7       | 15.4             | –                 | –   | –                 | 4.8              | –    | 42        |
| 8       | 3.05             | –                 | –   | –                 | 2.79             | –    | 42        |
| 9       | 5.1 <sup>a</sup> | –                 | –   | –                 | 5.5 <sup>b</sup> | –    | 44        |
| 10      | 5.1 <sup>a</sup> | –                 | –   | –                 | 5.2 <sup>b</sup> | –    | 45        |
| 11      | –                | –                 | –   | –                 | 5.9 <sup>c</sup> | –    | 46        |
| 13      | 7.4              | –                 | 7   | –                 | 5.8              | 4.9  | 47        |
| 14      | 9.9              | –                 | 8.3 | –                 | 6.1              | 4.9  | 47        |
| 15      | 12.2             | –                 | 9   | –                 | 6.1              | 4.7  | 47        |
| 16      | 7.1              | –                 | 7.3 | –                 | 5.1              | 4.5  | 47        |
| 17      | 10.6             | –                 | 7.5 | –                 | 5.7              | 4.5  | 47        |
| 18      | 12.3             | –                 | 9.2 | –                 | 6.6              | 5.5  | 47        |
| 19      | –                | –                 | –   | –                 | 6.4 <sup>c</sup> | –    | 48        |
| 20      | –                | –                 | –   | –                 | 5.4 <sup>c</sup> | –    | 48        |
| 21      | –                | –                 | –   | 7.20 <sup>c</sup> | –                | –    | 49        |
| 22      | –                | –                 | –   | 7.33 <sup>c</sup> | –                | –    | 49        |
| 23      | –                | –                 | –   | 6.65 <sup>c</sup> | –                | –    | 49        |
| 24      | –                | –                 | –   | 5.23 <sup>c</sup> | –                | –    | 49        |
| 25      | 3.67             | 4.84 <sup>d</sup> | –   | 6.47 <sup>e</sup> | –                | 3.34 | 50        |
| 26      | 4.39             | 6.31 <sup>d</sup> | –   | 7.17 <sup>e</sup> | –                | 4.80 | 50        |
| 27      | 2.09             | 3.94 <sup>d</sup> | –   | 5.01 <sup>e</sup> | –                | 2.65 | 50        |

<sup>a</sup> 40 °C, <sup>b</sup> 21 °C, <sup>c</sup> 25 °C, <sup>d</sup> 19.8 °C, <sup>e</sup> 19 °C

In addition to conjugation of multiple Gd<sup>III</sup>-containing units or incorporation of Gd<sup>III</sup> ions into proteins, conjugation of small molecules to Gd<sup>III</sup>-containing complexes is a method to increase relaxivity at ultra-high field strengths (Fig. 3, Table 2). Wang and co-workers reported myelin-specific Gd<sup>III</sup>-based contrast agents **9** and **10** that have higher relaxivities than **1** (3.9 mM<sup>-1</sup> s<sup>-1</sup> at 9.4 T and 25 °C) or **2** (4.1 mM<sup>-1</sup> s<sup>-1</sup> at 9.4 T and 25 °C) at ultra-high field strengths due to the increase in molecular weight resulting from conjugation with stilbene or coumarin derivatives (Table 2).<sup>44,45</sup> Chuang, Yang, and co-workers reported complex **11** as a potential tumour-targeting contrast agent that displays higher relaxivities than clinically approved contrast agents **1** or **2** at 9.4 T (Table 2).<sup>46</sup> Hagberg and co-workers reported a calcium ion sensitive contrast agent **12** that increased the relaxivity from 2.9 to 6.5 mM<sup>-1</sup> s<sup>-1</sup> at 37 °C and at 7 T as a function of the concentration of Ca<sup>2+</sup>.<sup>51</sup> Caravan and co-workers reported Gd<sup>III</sup>-DOTAAla-based complexes **13–18** that have rotational rates (1.7 × 10<sup>9</sup> to 6.7 × 10<sup>9</sup> s<sup>-1</sup>) and water-exchange rates that are near optimal at ultra-high field strengths.<sup>47</sup> Complexes **13–18** have higher relaxivities compared to clinically approved contrast agents **4** (3.0 mM<sup>-1</sup> s<sup>-1</sup> at 37 °C) and **5** (4.8 mM<sup>-1</sup> s<sup>-1</sup> at 37 °C) at 9.4 T (Table 1).<sup>47</sup> Bates and co-workers synthesized complexes **19** and **20** that display higher per-Gd relaxivities compared to clinically used contrast agents **1** and **2** at 9.4 T.<sup>48</sup> Complex **19** is seven coordinate (Gd<sup>III</sup> usually has a coordination number of nine); therefore, two remaining coordination sites can be occupied by water molecules to produce a water-coordination number of two. A higher water-coordination number and larger molecular weight caused complex **19** to have a higher relaxivity than clinically approved contrast agents. However, adjacent water-coordination sites are prone to coordination by bidentate anions like carbonates and phosphates leading to low relaxivities in biologically relevant media.<sup>52</sup> Complex **20**, relative to **19**, contains an octadentate ligand leaving only one site for water, but due to the higher molecular weight, complex **20** displays a slower rotational correlation rate leading to higher relaxivity than clinical contrast

agents at ultra-high fields. Angelovski and co-workers reported a series of Gd<sup>III</sup>-based complexes (**21–24**) that display higher relaxivities than clinically approved contrast agents **1** and **2** at 7 T and 25 °C (Table 2).<sup>49</sup>

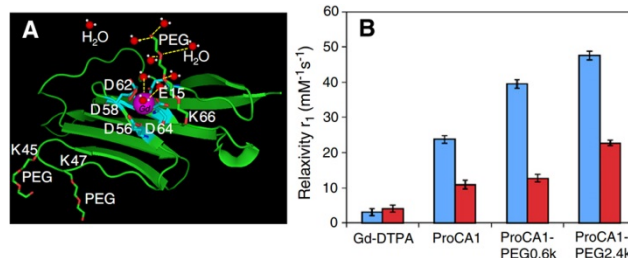


**Fig. 4** (A) Model of PEGylated ProCA1 metalated with Gd<sup>III</sup> (pink: Gd<sup>III</sup>; blue: metalation site; green: ProCA1; red and green: PEG; yellow and red: water); (B) Relaxivity values of ProCA1 and PEGylated-ProCA1 (blue at 3 T and red at 9.4 T). Reprinted from the *Journal of Inorganic Biochemistry*, **107**, S. Li, J. Jiang, J. Zou, J. Qiao, S. Xue, L. Wei, R. Long, L. Wang, A. Castiblanco, N. White, J. Ngo, H. Mao, Z.-R. Liu and J. J. Yang, PEGylation of Protein-Based MRI Contrast Agents Improves Relaxivities and Biocompatibilities, 111–118, Copyright 2013, with permission from Elsevier.

The examples in this section demonstrate the influence of rotational correlation rate and the number of coordinated water molecules on relaxivity at ultra-high field strengths. Although these examples show increases in relaxivity at ultra-high fields compared to clinically approved T<sub>1</sub>-shortening contrast agents, the relaxivities per metal ion for complexes **7–24** are only slightly larger than the relaxivities of clinically approved T<sub>1</sub>-shortening contrast agents at ultra-high field strengths and 37 °C. This small increase has generated interest in alternatives to Gd<sup>III</sup>-based contrast agents, and these agents are described in the remaining sections of this review.

## (2) Eu<sup>II</sup>-Containing Cryptates as T<sub>1</sub>-Shortening Agents

Eu<sup>II</sup>-containing cryptates have been explored as an alternate to Gd<sup>III</sup>-containing contrast agents. Eu<sup>II</sup> is isoelectronic with Gd<sup>III</sup>, and the molecular parameters that influence the relaxivity of Gd<sup>III</sup> influence Eu<sup>II</sup> in similar fashion.<sup>53</sup> However, the larger radius (117 pm for Eu<sup>II</sup> vs 93.8 pm for Gd<sup>III</sup>)<sup>54</sup> and lower charge of Eu<sup>II</sup> allow the ion to have faster water-exchange rates than Gd<sup>III</sup>.<sup>55</sup> Further, Eu<sup>II</sup>-containing cryptates have two coordinated water molecules because Eu<sup>II</sup> is large enough to have a coordination number of ten.<sup>55</sup>

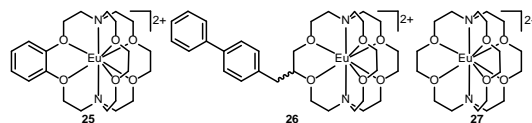


**Fig. 5** Eu<sup>II</sup>-containing cryptates (**25–27**) (coordinated water molecules and counter ions are not shown for clarity).

Allen and co-workers reported a series of Eu<sup>II</sup>-containing cryptates **25–27** (Fig. 5) that are more efficient contrast agents than **2** (3.7 mM<sup>-1</sup> s<sup>-1</sup> at 7 T and 19 °C) at ultra-high field strengths (Table 2).<sup>50</sup> The higher relaxivities of Eu<sup>II</sup>-containing cryptates relative to **2** at ultra-high fields are due to the ability to accommodate two water molecules in the inner sphere, the increase in water-exchange rates, and changes in rotational correlation rates compared to **2**.<sup>50,56</sup> The differences in relaxivities among different cryptates arise mainly from the changes in the rotational correlation rates that are proportional to molecular weight differences.<sup>50</sup> Eu<sup>II</sup>-

## MINIREVIEW

containing cryptates that display higher relaxivities than Gd<sup>III</sup>-based contrast agents at ultra-high field strengths are potential alternatives to Gd<sup>III</sup>-based contrast agents in  $T_1$ -weighted imaging. One of the current limitations of Eu<sup>III</sup>-containing complexes is their tendency to oxidize to Eu<sup>IV</sup> in the presence of air. While some work has been done to overcome this effect,<sup>57,58</sup> further investigations are required to understand the *in vivo* outcomes of the oxidized products.

(3) <sup>19</sup>F-MRI Agents

<sup>19</sup>F-MRI works similarly to <sup>1</sup>H-MRI, but instruments map the relaxation of <sup>19</sup>F (part of the contrast agent), as opposed to <sup>1</sup>H (part of the environment surrounding the contrast agent), to produce images. One advantage of using <sup>19</sup>F instead of <sup>1</sup>H is the lack of background signal (<sup>19</sup>F is not found in appreciable amounts in humans outside of teeth).<sup>59</sup> The <sup>19</sup>F nuclei have 100% natural abundance and 83% NMR sensitivity relative to <sup>1</sup>H, making <sup>19</sup>F-MRI an active area of research.<sup>59–62</sup> Contrast enhancement with <sup>19</sup>F-MRI is increased with the use of ultra-high field strengths because signal intensity is proportional to field strength. This increase in signal intensity results in lower amounts of fluorinated agents being needed to obtain MR images (usually <sup>19</sup>F-MRI requires concentrations of <sup>19</sup>F to be in the millimolar range for imaging).<sup>63</sup> Because of the low sensitivity for detection of <sup>19</sup>F by MRI, two strategies have been reported to increase the sensitivity of <sup>19</sup>F-MRI. The first strategy is to incorporate as many <sup>19</sup>F atoms into the structure as possible, and the other strategy is to incorporate a lanthanide ion to influence the relaxation rate of nearby <sup>19</sup>F nuclei.<sup>63</sup> Increases in relaxation rates also allow for faster acquisition rates in imaging.<sup>64</sup>

A series of <sup>19</sup>F-labeled lanthanide-based contrast agents (28–32, Fig. 6) were reported by Blamire and co-workers.<sup>63</sup> They used phosphonate-based 1,4,7,10-tetraazacyclododecane-1,4,7-triacetate (DO3A)-type ligands that were metalated with different lanthanide ions. Selection of the lanthanide ion and the imaging parameters were found to be key factors for using these agents for ultra-high field applications. Blamire and co-workers also reported that Dy<sup>III</sup>-containing complex 29 provided the highest relaxation rates of the group at 4.7, 7.0, and 9.4 T (Table 3). Due to the high contrast gained from incorporation of Dy<sup>III</sup>, micromolar concentrations (20 μM) of 29 were detectable in phantom images compared to the typical sensitivity of <sup>19</sup>F-MRI that is usually in the millimolar range.<sup>63</sup> Incorporation of lanthanide ions have been reported by Parker and co-workers with a phosphonate-based Dy<sup>III</sup>-DO3A conjugated to chitosan (a linear polysaccharide) to result in complex 33 (Fig. 6) that shows comparable longitudinal relaxation rates to complex 29 at 4.7 and 9.4 T (Table 3).<sup>65</sup> Conjugation of chitosan improved the retention time of complex 33 *in vivo* leading to lower amounts of the contrast agent being needed for imaging.

Faber and co-workers reported complexes 34–37.<sup>66</sup> Complexes 34 and 35 displayed higher relaxation rates (Table 3) and signal-to-noise ratios than complexes 36 and 37 at 9.4 T, leading to higher sensitivities. Kikuchi and co-workers reported contrast agents 38 and 39 that show decreased relaxation rates in the presence of enzymes.<sup>67,68</sup> Complexes 38 and 39 react with β-galactosidase and β-lactamase, respectively, resulting in detachment of the <sup>19</sup>F-containing moiety from the metal complex and a slowing of relaxation rates.

Contrast agents based on <sup>19</sup>F are important because of the near zero background signal and the high natural abundance of

the <sup>19</sup>F nucleus. Ultra-high field strengths enhance the signal intensity of <sup>19</sup>F-based contrast agents, and <sup>19</sup>F-based agents are potentially useful in monitoring changes in biological environments, but the low sensitivity of <sup>19</sup>F-based agents limits their applicability and justifies further investigation in this area.

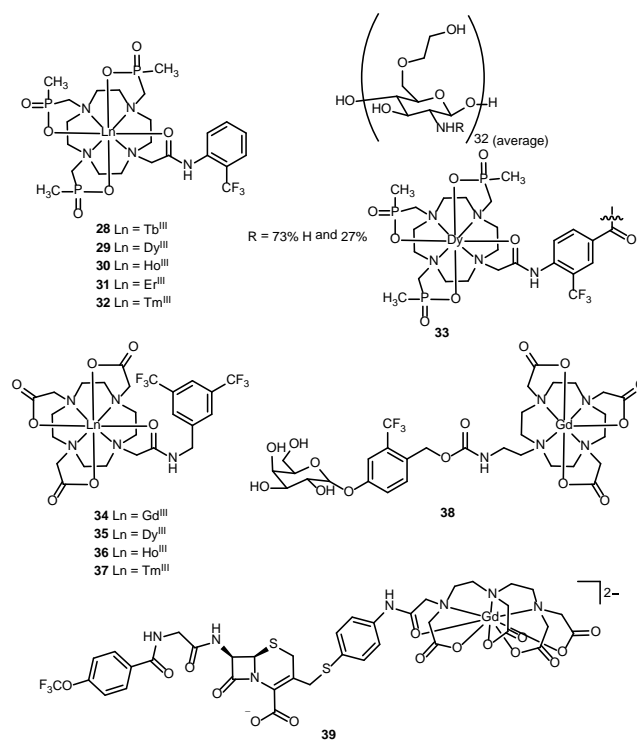


Fig. 6 Ln<sup>III</sup>-based contrast agents 28–39 for <sup>19</sup>F-MRI.

Table 3 Longitudinal relaxation rates (s<sup>-1</sup>) of <sup>19</sup>F-based contrast agents at 25 °C and 4.7, 7, and 9.4 T.

| Complex | 4.7              | 7.0   | 9.4              | Reference |
|---------|------------------|-------|------------------|-----------|
| 28      | 84.0             | 113.0 | 146.6            | 63        |
| 29      | 103.8            | 143.9 | 184.8            | 63        |
| 30      | 58.1             | 88.0  | 120.1            | 63        |
| 31      | 71.1             | 90.9  | 108.9            | 63        |
| 32      | 46.6             | 56.4  | 63.3             | 63        |
| 33      | 108 <sup>a</sup> | –     | 183 <sup>a</sup> | 65        |
| 34      | –                | –     | 694              | 66        |
| 35      | –                | –     | 160              | 66        |
| 36      | –                | –     | 69.9             | 66        |
| 37      | –                | –     | 130              | 66        |

<sup>a</sup> 22 °C

## (4) Chemical Exchange Saturation Transfer Agents

In addition to  $T_1$ -weighted imaging used for <sup>1</sup>H and <sup>19</sup>F, another type of MRI experiment is chemical exchange saturation transfer (CEST) that uses proton transfer between two chemically distinct proton pools to produce images. In CEST, one pool is saturated by a radio frequency pulse, and chemical exchange of saturated protons with the bulk water decreases the signal intensity of the bulk water. The difference in the signal intensities before and after exchange can be mapped to produce images.<sup>69</sup> This imaging modality can be used to monitor changes in pH, temperature, and analyte concentration (anions and metal ions).<sup>70,71</sup> At ultra-high field strengths, high signal intensities for CEST can be achieved

1 because, as with  $^{19}\text{F}$ , signal intensity depends on the field  
2 strength.<sup>24,69</sup> Also, the separation between signals from CEST  
3 agents and bulk water increases with field strength. When the  
4 signal from a CEST agent is close ( $<5$  ppm) to the bulk water  
5 signal, saturation pulses can excite protons in both pools  
6 decreasing the signal intensity (CEST effect) before the proton  
7 exchange can take place. Interference with saturation  
8 frequency can be reduced by making the exchangeable pool  
9 appear farther from the bulk water signal ( $>5$  ppm). Large  
10 frequency differences between the two pools also allow the  
11 use of relatively fast proton-exchange rates (for CEST agents,  
12 proton-exchange rates above  $10^3$  s $^{-1}$  are considered fast)  
13 instead of the typically desired slow exchange rates ( $\sim 2 \times 10^3$   
14 s $^{-1}$ ).<sup>72,73</sup> This range of proton-exchange rates allows the use of  
15 CEST agents, including lanthanide-based paramagnetic CEST  
16 (PARACEST) agents that usually have intermediate to fast  
17 proton-exchange rates. PARACEST agents are mainly  
18 paramagnetic metal complexes that contain exchangeable  
19 protons. Because of the paramagnetic center, the exchangeable  
20 proton signal is shifted farther from the bulk water signal than  
21 in the case of CEST agents. This shift from the bulk water  
22 signal increases the sensitivity of the PARACEST agent. This  
23 shifting is especially important *in vivo* where there are many  
24 endogenous exchangeable protons. The following section  
25 describes the recent examples of CEST and PARACEST  
26 agents.

27 A series of thymidine-based (40–43, Fig. 7) CEST agents  
28 have been reported by Gilad and co-workers at 3 and 11.7 T.<sup>74</sup>  
29 For compounds 40 and 41, distinguishable peaks ( $\geq 5$  ppm  
30 from the bulk water signal) for amide protons were not  
31 observed at 3 T due to fast proton-exchange rates ( $\geq 3.7 \times 10^3$   
32 s $^{-1}$ ), but at 11.7 T both 40 and 41 showed peaks distinct from  
33 the bulk water peaks. Compounds 42 and 43 showed signals  
34 for amide protons 5 ppm from the bulk water signal at both  
35 field strengths, but the peaks at 11.7 T were prominent  
36 because of the slow proton-exchange rate ( $\leq 1.7 \times 10^3$  s $^{-1}$ ).<sup>74</sup>  
37 CEST agents that show greater shifts from bulk water than  
38 thymidine-based agents have been reported by Pomper,  
39 McMahan, and co-workers.<sup>75</sup> These agents contain salicylic  
40 acid or its analogues (44–50, Fig. 7). Compounds 44–50  
41 displayed shifts of 8.7–10.8 ppm from bulk water at 11.7 T at  
42 pH 7 and 37 °C. Compound 51 (Fig. 7) has been reported by  
43 Bulte, McMahan, and co-workers, and they showed that CEST  
44 activity detected with  $^{19}\text{F}$ -NMR can be used to detect Ca $^{2+}$   
45 selectively in the presence of Mg $^{2+}$  and Zn $^{2+}$  (Ca $^{2+}$  results in  
46 slow exchange rates compared to Mg $^{2+}$  and Zn $^{2+}$ ).<sup>76</sup> The Ca $^{2+}$ -  
47 containing complex shows 6.2 ppm shift from the free ligand.  
48 The fluorinated free ligands and metal-bound ligands were  
49 used as the exchangeable nuclei and  $^{19}\text{F}$ -MRI was used to  
50 observe CEST activity.<sup>76</sup>

51 A series of Ln $^{III}$ - and transition metal-based PARACEST  
52 complexes (52–67, Fig. 7) were reported by Morrow and co-  
53 workers.<sup>71,77–83</sup> Complex 52 displayed changes in CEST effect  
54 in response to the presence or absence of the biologically  
55 important anions lactate, citrate, and phosphate at 11.7 T and  
56 pH 6.5.<sup>71</sup> Complex 52 showed a chemical shift of 6 ppm from  
57 the bulk water signal in the CEST spectrum due to  
58 exchangeable alcohol protons. The addition of lactate and  
59 acetate shifted the peak to 7 ppm, and in the presence of  
60 citrate, the peak shifted to 8 ppm. Complexes 53 and 54  
displayed changes in CEST effect in response to the  
interaction of phosphate diesters at neutral pH values.<sup>77</sup>  
Complex 53 showed a CEST signal around 5 ppm with respect  
to the bulk water when one equivalent of diethyl phosphate

was added. Similarly, complex 54 displayed a CEST signal  
around 20 ppm with respect to bulk water when diethyl  
phosphate was added. Fe $^{II}$ -containing PARACEST agents 55  
and 56 displayed changes in CEST effect with respect to pH.<sup>81</sup>  
Complex 55 showed a CEST signal at 54 ppm, and the  
intensity of the peak decreased with increasing pH from 6.4 to  
7.3 at 11.7 T and at 37 °C. The signal intensity of complex 56  
at 50 ppm from the bulk water increases in intensity with  
increasing pH from 6.8 to 7.6.<sup>81</sup> Complexes 58 and 61 showed  
69 and 6 ppm shifts, respectively, from bulk water at 9.4 T.<sup>78</sup>  
The smaller shift observed with complex 61 compared to 58  
was attributed to the slower proton-exchange rates of anilines  
compared to amides.

Complexes 59, 62, and 64 are Ni $^{II}$ -containing PARACEST  
agents. The most intense CEST effect of the three was  
observed for complex 64 at 76 ppm from bulk water at 11.7  
T.<sup>79</sup> Complexes 59 and 62 showed CEST effects at 76 and 72  
ppm, respectively, from bulk water at 11.7 T, but the effects  
were 2–4-fold lower than that of complex 64.<sup>79</sup> A series of  
Co $^{II}$ -containing complexes 57, 60, 63, 65, and 67 have also  
been reported.<sup>80,82</sup> The redox active complex 67 was studied at  
11.7 T as a potential probe to map *in vivo* oxygen levels.<sup>80</sup>  
Complex 67 with a CEST effect at 135 ppm from bulk water  
becomes CEST silent in the presence of oxygen.<sup>80</sup> Complexes  
57, 60, 63, and 65 displayed pH sensitive CEST effects in the  
pH range 6.5–7.5.<sup>82</sup> CEST signals for complexes 57 and 60  
were at 45 and 32 ppm, respectively, and the signals for  
complex 65 were at –19 and 59 ppm.<sup>82</sup> Complex 63 displayed  
four CEST signals (112, 95, 54, and 45 ppm), and all shifts  
were measured at 11.7 T and 37 °C.<sup>82</sup> Complexes 64–66 were  
reported for their pH sensitive CEST effects between pH 6.5  
and 7.7.<sup>83</sup> Complexes 64–66 displayed CEST signals at 72, 59,  
and 92 ppm, respectively, with CEST effects ranging from 25  
to 39%.<sup>83</sup>

Kovacs and co-workers reported a Eu $^{III}$ -containing  
PARACEST agent (68, Fig. 7) that can be activated by a redox  
reaction.<sup>84</sup> The complex contained nitroxide free radicals that  
slow the longitudinal relaxation rates of amide protons, but  
after oxidation in the presence of ascorbic acid, nitroxide  
radicals convert to nitroxide, resulting in an increase of the  
CEST effect to 20% at 9.4 T and 50 ppm from the bulk  
water.<sup>84</sup> Coman, Hyder, and co-workers reported a  
temperature-sensitive Eu $^{III}$ -based PARACEST agent (69, Fig.  
7) that enhanced the intensity of the CEST effect between 25  
and 40 °C and decreased the intensity above 40 °C at 11.7 T  
due to increased water-exchange rate at high temperature.<sup>85</sup>  
Angelovski, Tóth, and co-workers reported calcium-ion-  
responsive PARACEST agents 70 and 71 that displayed a 60%  
CEST effect at 41 ppm and a 35% effect at –11 ppm,  
respectively, due to the exchange of amide protons in the  
absence of calcium ions (11.7 T, 37 °C, and pH 7.4).<sup>86</sup> The  
addition of calcium ions decreased the signal intensities due  
to the slowing of amide proton exchange. Durand, Tóth, and co-  
workers reported pH responsive PARACEST agents 72 and 73  
that displayed CEST signals at about –25 ppm from bulk water  
at 11.7 T and 37 °C.<sup>87</sup> For complex 73, a decrease in CEST  
effect from 65 to 15% was observed upon increasing the pH  
from 6.3 to 9.<sup>87</sup> Kotek and co-workers also reported pH  
responsive PARACEST agents.<sup>88</sup> Complexes 74 and 75  
displayed changes in signal intensities over the pH range of 6–  
8. Complex 74 displayed two peaks at 19.5 and 34 ppm (25 °C  
and pH 7.67), and complex 75 displayed CEST signals at 42  
and 89 ppm (25 °C and pH 7.4) at 7.05 T.<sup>88</sup>





complex **83**.<sup>91–94</sup> Complex **80** reacts with esterases to produce hydrocourmarins and amine-functionalized metal complexes that in turn produce a CEST signal at 12 ppm (14 T, 37 °C, and pH 7.4).<sup>91</sup> Complex **81** reacts with the enzyme transglutaminase to form a covalent bond between the metal complex and albumin, decreasing the CEST effect caused by albumin at 4.6 ppm and leading to the appearance of a new signal at –9.2 ppm (14 T, 37 °C, and pH 7.4).<sup>92</sup> Complex **82**, on the other hand, becomes CEST silent after reacting with the enzyme urokinase (before the enzyme reaction, the metal complex displays a signal at –54.1 ppm at 7.05 T and 37 °C).<sup>93</sup> Complex **83** displayed CEST signals at –9.8 and 9.75 ppm, and the ratio between the intensities of these signals changes linearly with respect to changes in pH between 6.0 and 7.6 (14 T and 38.3 °C).<sup>94</sup> Hudson and co-workers synthesized a series of PARACEST agents **84–87** to study the CEST effect.<sup>95,96</sup> The CEST effects of complexes **84–86** were greater than 18%, whereas the analogous Tm<sup>III</sup>- and Dy<sup>III</sup>-containing complexes produced CEST effects less than 18%.<sup>95</sup> Complex **87** also has been studied for its pH responsive CEST effect.<sup>96</sup> This complex produced a six-fold increase in CEST effect upon changing pH from 6.5 to 7.0 (9.4 T and 37 °C).<sup>96</sup>

As demonstrated by the examples in this section, CEST agents can be effectively used at ultra-high field strengths to monitor biologically relevant environmental changes. Although CEST agents are versatile in terms of monitoring changes in environments, they suffer from low sensitivity which is a prime area for research.

## Summary and Conclusions

Ultra-high field strength MRI is capable of generating images with high signal-to-noise ratios potentially making detection of pathologies more accurate. Contrast agents have been used to achieve high contrast between pathologies and the surrounding environment, but clinically approved contrast agents are less efficient at ultra-high field strengths relative to low field strengths. Optimization of molecular parameters to increase the efficiency of Gd<sup>III</sup>-based contrast agents at ultra-high fields and other non-Gd<sup>III</sup>-based strategies have been reported and are being investigated by a number of research groups. There is opportunity for different types of contrast agents to be used in ultra-high field applications, but further research is needed for all of these strategies. A possible future for ultra-high field contrast agents will likely consist of a combination of these strategies.

## Acknowledgements

The authors acknowledge the National Institutes of Health (R01EB013663) for support and Levi Ekanger for assistance with Fig. 4.

## Notes and references

<sup>a</sup> Department of Chemistry, Wayne State University, 5101 Cass Avenue, Detroit, MI 48202, USA. E-mail: mallen@chem.wayne.edu; Fax: 1 313 577 8822; Tel: 1 313 577 2070

- 1 J. H. Duyn, *NeuroImage*, 2012, **62**, 1241.
- 2 E. Moser, F. Stahlberg, M. E. Ladd and S. Trattnig, *NMR Biomed.*, 2012, **25**, 695.
- 3 O. Kraff, A. Fischer, A. M. Nagel, C. Mönninghoff and M. E. Ladd, *J. Magn. Reson. Imaging*, 2014, DOI: 10.1002/jmri.24573.
- 4 E. Moser, *World J. Radiol.*, 2010, **2**, 37.

- 5 K. Kollia, S. Maderwald, N. Putzki, M. Schlamann, J. M. Theysohn, O. Kraff, M. E. Ladd, M. Frosting and I. Wanke, *Am. J. Neuroradiol.*, 2009, **30**, 699.
- 6 R. Beisteiner, S. Robinson, M. Wurnig, M. Hilbert, K. Merksa, J. Rath, I. Höllniger, N. Kilinger, C. Marosi, S. Trattnig and A. Geißler, *NeuroImage*, 2011, **57**, 1015.
- 7 C. Moeninghoff, S. Maderwald, J. M. Theysohn, O. Kraff, M. E. Ladd, N. E. Hindy, J. van de Nes, M. Frosting and I. Wanke, *Eur. Radiol.*, 2010, **20**, 704.
- 8 A. G. van der Kolk, J. Hendrikse, J. J. M. Zwanenburg, F. Visser and P. R. Luijten, *Eur. J. Radiol.* 2013, **82**, 708.
- 9 D. Li, J. Zheng and H.-J. Weinmann, *Radiology*, 2001, **218**, 670.
- 10 S. Huang, C. Liu, G. Dai, Y. R. Kim and B. R. Rosen, *NeuroImage*, 2009, **46**, 589.
- 11 A. J. L. Villaraza, A. Bumb and M. W. Brechbiel, *Chem. Rev.*, 2010, **110**, 2921.
- 12 C. Tu, E. A. Osborne and Y. Louie, *Ann. Biomed. Eng.*, 2011, **39**, 1335.
- 13 L. Helm, *Future Med. Chem.*, 2010, **2**, 385.
- 14 G. E. Hagberg and K. Sheffler, *Contrast Media Mol. Imaging*, 2013, **8**, 456.
- 15 O. C. Richardson, M. L. J. Scott, S. F. Tanner, J. C. Waterton and D. L. Buckley, *Magn. Reson. Med.*, 2012, **68**, 1234.
- 16 J. T. Rosenberg, J. M. Kogot, C. Ridel, G. F. Strouse and S. C. Grant, *Proc. Intl. Soc. Magn. Reson. Med.*, 2009, **17**, 921.
- 17 S. Xue, J. Qiao, F. Pu, M. Cameron and J. J. Yang, *Nanobiotechnol.* 2013, **5**, 163.
- 18 E. Terreno, D. D. Castelli, A. Viale and S. Aime, *Chem. Rev.*, 2010, **110**, 3019.
- 19 M. C. Heffern, L. M. Matosziuk and T. J. Meade, *Chem. Rev.*, 2014, **114**, 4496.
- 20 J. Garcia and M. J. Allen, *Eur. J. Inorg. Chem.* 2012, **2012**, 4550.
- 21 V. Hsieh and A. Jasanoff, *ACS Chem. Neurosci.*, 2012, **3**, 593.
- 22 E. T. Ahrens and J. Zhong, *NMR Biomed.* 2013, **26**, 860.
- 23 K. W. Y. Chan, J. W. M. Bulte and M. T. McMahon, *WIREs Nanomed. Nanobiotechnol.*, 2014, **6**, 111.
- 24 G. Liu, X. Song, K. W. Y. Chan and M. T. McMahon, *NMR Biomed.*, 2013, **26**, 810.
- 25 M. Srinivas, A. Heerschap, E. T. Ahrens, C. G. Figdor and I. J. M. de Vries, *Trends Biotechnol.*, 2010, **28**, 363.
- 26 W. Xu, K. Kattel, J. Y. Park, Y. Chang, T. J. Kim and G. H. Lee, *Phys. Chem. Chem. Phys.*, 2012, **14**, 12687.
- 27 J. Gallo, N. J. Long and E. O. Aboagye, *Chem. Soc. Rev.*, 2013, **42**, 7816.
- 28 L. T. Quentin, S. Hervé and D. Marie-Hélène, *Nanotechnology Reviews*, 2013, **2**, 125.
- 29 D. D. Castelli, E. Terreno, D. Longo and S. Aime, *NMR Biomed.* 2013, **26**, 839.
- 30 L. Shan, A. Chopra, K. Leung, W. C. Eckelman and A. E. Menkens, *J. Nanopart. Res.*, 2012, **14**, 1122.
- 31 R. Srikanth, A. Upendran and R. Kannan, *WIREs Nanomed. Nanobiotechnol.*, 2014, **6**, 245.
- 32 M. Rohrer, H. Bauer, J. Mintorovitch, M. Requardt and H.-J. Weinmann, *Invest. Radiol.*, 2005, **40**, 715.
- 33 I. M. Noebauer-Huhmann, P. Szomolanyi, V. Juras, O. Kraff, M. E. Ladd and S. Trattnig, *Invest. Radiol.*, 2010, **45**, 554.

## MINIREVIEW

- 1  
2  
3  
4  
5  
6  
7  
8  
9  
10  
11  
12  
13  
14  
15  
16  
17  
18  
19  
20  
21  
22  
23  
24  
25  
26  
27  
28  
29  
30  
31  
32  
33  
34  
35  
36  
37  
38  
39  
40  
41  
42  
43  
44  
45  
46  
47  
48  
49  
50  
51  
52  
53  
54  
55  
56  
57  
58  
59  
60
- 34 P. Caravan and Z. Zhang, *Eur. J. Inorg. Chem.*, 2012, 1916.
- 35 L. M. Manus, R. C. Strauch, A. H. Hung, A. L. Eckermann and T. J. Meade, *Anal. Chem.*, 2012, **84**, 6278.
- 36 P. Caravan, C. T. Farrar, L. Frullano and R. Uppal, *Contrast Media Mol. Imaging*, 2009, **4**, 89.
- 37 P. Caravan, J. J. Ellison, T. J. McMurry and R. B. Lauffer, *Chem. Rev.*, 1999, **99**, 2293.
- 38 M. Polasek and P. Caravan, *Inorg. Chem.* 2013, **52**, 4084.
- 39 J. M. Bryson, J. W. Reineke and T. M. Reineke, *Macromolecules*, 2012, **45**, 8939.
- 40 A. Kundu, A. H. Peterlik, H. M. Krssak, A. K. Bytzek, I. Pashkunova-Martic, I. V. B. Arion, T. H. Helbich and B. K. Keppler, *J. Inorg. Biochem.*, 2011, **105**, 250.
- 41 P. D. Garimella, A. Datta, D. W. Romanini, K. N. Raymond and M. B. Francis, *J. Am. Chem. Soc.* 2011, **133**, 14704.
- 42 D. J. Mastarone, V. S. R. Harrison, A. L. Eckermann, G. Parigi, C. Luchinat and T. J. Meade, *J. Am. Chem. Soc.*, 2011, **133**, 5329.
- 43 S. Li, J. Jiang, J. Zou, J. Qiao, S. Xue, L. Wei, R. Long, L. Wang, A. Castiblanco, N. White, J. Ngo, H. Mao, Z.-R. Liu and J. J. Yang, *J. Inorg. Biochem.*, 2012, **107**, 111.
- 44 L. Frullano, J. Zhu, R. H. Miller and Y. Wang, *J. Med. Chem.* 2013, **56**, 1629.
- 45 L. Frullano, C. Wang, R. H. Miller and Y. Wang, *J. Am. Chem. Soc.*, 2011, **133**, 1611.
- 46 P. Chandrasekharan, C.-X. Yong, Z. Poh, T. He, Z. He, S. Liu, E. G. Robins, K.-H. Chuang and C.-T. Yang, *Biomaterials*, 2012, **33**, 9225.
- 47 E. Boros, M. Polasek, Z. Zhang and P. Caravan, *J. Am. Chem. Soc.* 2012, **134**, 19858.
- 48 K. Kittigowittana, C.-T. Yang, W. C. Cheah, K.-H. Chuang, C.-Y. Tuang, Y.-T. Chang, X. Golay and R. W. Bates, *Chem. Med. Chem.*, 2011, **6**, 781.
- 49 M. P. Placidi, J. Engelmann, L. S. Natrajan, N. K. Logothetis and G. Angelovsky, *Chem. Commun.*, 2011, **47**, 11534.
- 50 J. Garcia, J. Neelavalli, E. M. Haacke and M. J. Allen, *Chem. Commun.*, 2011, **47**, 12858.
- 51 G. E. Hagberg, I. Mamedov, A. Power, M. Beyerlein, H. Merkle, V. G. Kiselev, K. Dhingra, V. Kubiček, G. Angelovsky and N. K. Logothetis, *Contrast Media Mol. Imaging*, 2014, **9**, 71.
- 52 S. Silvério, S. Torres, A. F. Martins, J. A. Martins, J. P. André, L. Helm, M. I. M. Prata, A. C. Santos and C. F. G. C. Geraldés, *Dalton Trans.*, 2009, 4656.
- 53 J. Garcia and M. J. Allen, *Inorg. Chim. Acta*, 2012, **393**, 324.
- 54 N. N. Greenwood and A. Earnshaw, *Chemistry of the Elements*, Elsevier Butterworth-Heinemann, Burlington, 2nd edn., 2005, p. 1233.
- 55 L. Burai, R. Scopelliti and É. Tóth, *Chem. Commun.*, 2002, 2366.
- 56 J. Garcia, A. N. W. Kuda-Wedagedara and M. J. Allen, *Eur. J. Inorg. Chem.*, 2012, **2012**, 2135.
- 57 N.-D. H. Gamage, Y. Mei, J. Garcia and M. J. Allen, *Angew. Chem. Int. Ed.*, 2010, **49**, 8923.
- 58 M. Gál, F. Kielar, R. Sokolová, S. Ramešová and V. Kolivoška, *Eur. J. Inorg. Chem.*, 2013, **2013**, 3217.
- 59 P. Harvey, K. H. Chalmers, E. D. Luca, A. Mishra and D. Parker, *Chem. Eur. J.*, 2012, **18**, 8748.
- 60 H. Matsushita, S. Mizukami, Y. Mori, F. Sugihara, M. Shirakawa, Y. Yoshioka and K. Kikuchi, *Chem. Bio. Chem.* 2012, **13**, 1579.
- 61 J. Ruiz-Cabello, B. P. Barnett, P. A. Bottomley and J. W. M. Bulte, *NMR Biomed.*, 2011, **24**, 114.
- 62 J. Chen, G. M. Lanza and S. A. Wickline, *WIREs Nanomed. Nanobiotechnol.*, 2010, **2**, 431.
- 63 K. H. Chalmers, A. M. Kenwright, D. Parker and A. M. Blamire, *Magn. Reson. Med.* 2011, **66**, 931.
- 64 K. H. Chalmers, M. Botta and D. Parker, *Dalton Trans.*, 2011, **40**, 904.
- 65 E. D. Luca, P. Harvey, K. H. Chalmers, A. Mishra, P. K. Senanayake, J. I. Wilson, M. Botta, M. Fekete, A. M. Blamire and D. Parker, *J. Biol. Inorg. Chem.*, 2014, **19**, 215.
- 66 F. Schmid, C. Höltke, D. Parker and C. Faber, *Magn. Reson. Med.*, 2013, **69**, 1056.
- 67 S. Mizukami, H. Matsushita, R. Takikawa, F. Sugihara, M. Shirakawa and K. Kikuchi, *Chem. Sci.*, 2011, **2**, 1151.
- 68 H. Matsushita, S. Mizukami, Y. Mori, F. Sugihara, M. Shirakawa, Y. Yoshioka and K. Kikuchi, *Chem. Bio. Chem.*, 2012, **13**, 1579.
- 69 P. C. M. van Zijl and N. N. Yadav, *Magn. Reson. Med.*, 2011, **65**, 927.
- 70 S. J. Dorazio, A. O. Olatunde, P. B. Tsitovich and J. R. Morrow, *J. Biol. Inorg. Chem.*, 2014, **19**, 191.
- 71 J. Hammell, L. Buttarazzi, C.-H. Huang and J. R. Morrow, *Inorg. Chem.* 2011, **50**, 4857.
- 72 E. Vinogradov, A. D. Sherry and R. E. Lenkinski, *J. Magn. Reson.*, 2013, **229**, 155.
- 73 A. N. Dula, S. A. Smith and J. C. Gore, *J. Neuroimaging*, 2013, **23**, 526.
- 74 A. Bar-Shir, G. Liu, Y. Liang, N. N. Yadav, M. T. McMahon, P. Walczak, S. Nimmagadda, M. G. Pomper, K. A. Tallman, M. M. Greenberg, P. C. M. van Zijl, J. W. M. Bulte and A. A. Gilad, *J. Am. Chem. Soc.*, 2013, **135**, 1617.
- 75 X. Yang, X. Song, Y. Li, G. Liu, S. R. Banerjee, M. G. Pomper and M. T. McMahon, *Angew. Chem. Int. Ed.*, 2013, **52**, 8116.
- 76 A. Bar-Shir, A. A. Gilad, K. W. Y. Chan, G. Liu, P. C. M. van Zijl, J. W. M. Bulte and M. T. McMahon, *J. Am. Chem. Soc.* 2013, **135**, 12164.
- 77 C.-H. Huang, J. Hammell, S. J. Ratnakar, A. D. Sherry and J. R. Morrow, *Inorg. Chem.*, 2010, **49**, 5963.
- 78 S. J. Dorazio, P. B. Tsitovich, K. E. Sifers, J. A. Sperryak and J. R. Morrow, *J. Am. Chem. Soc.*, 2011, **133**, 14154.
- 79 A. O. Olatunde, S. J. Dorazio, J. A. Sperryak and J. R. Morrow, *J. Am. Chem. Soc.*, 2012, **134**, 18503.
- 80 P. B. Tsitovich, J. A. Sperryak and J. R. Morrow, *Angew. Chem. Int. Ed.*, 2013, **52**, 13997.
- 81 S. J. Dorazio and J. R. Morrow, *Inorg. Chem.*, 2012, **51**, 7448.
- 82 S. J. Dorazio, A. O. Olatunde, J. A. Sperryak and J. Morrow, *Chem. Commun.*, 2013, **49**, 10025.
- 83 A. O. Olatunde, J. M. Cox, M. D. Daddario, J. A. Sperryak, J. B. Benedict and J. R. Morrow, *Inorg. Chem.*, 2014, DOI: 10.1021/ic5006083.
- 84 S. J. Ratnakar, T. C. Soesbe, L. L. Lumata, Q. N. Do, S. Viswanathan, C.-Y. Lin, A. D. Sherry and Z. Kovacks, *J. Am. Chem. Soc.*, 2013, **135**, 14904.
- 85 D. Coman, G. E. Kiefer, D. L. Rothman, A. D. Sherry and F. Hyder, *NMR Biomed.*, 2011, **24**, 1216.
- 86 G. Angelovski, T. Chauvin, R. Pohmann, N. K. Logothetis and É. Tóth, *Bioorg. Med. Chem.*, 2011, **19**, 1097.

- 1  
2  
3  
4  
5  
6  
7  
8  
9  
10  
11  
12  
13  
14  
15  
16  
17  
18  
19  
20  
21  
22  
23  
24  
25  
26  
27  
28  
29  
30  
31  
32  
33  
34  
35  
36  
37  
38  
39  
40  
41  
42  
43  
44  
45  
46  
47  
48  
49  
50  
51  
52  
53  
54  
55  
56  
57  
58  
59  
60
- 87 T. Chauvin, S. Torres, R. Rosseto, J. Kotek, B. Badet, P. Durand and  
É. Tóth, *Chem. Eur. J.*, 2012, **18**, 1408.
- 88 T. Krchová, J. Kotek, D. Jiráček, J. Havlíčková, I. Císařová and P.  
Hermann, *Dalton Trans.*, 2013, **42**, 15735.
- 89 G. Ferrauto, D. D. Castelli, E. Terreno and S. Aime, *Magn. Reson.  
Med.*, 2013, **69**, 1703.
- 90 I.-R. Jeon, J. G. Park, C. R. Haney and T. D. Harris, *Chem. Sci.*, 2014,  
**5**, 2461.
- 91 Y. Li, V. R. Sheth, G. Liu and M. D. Pagel, *Contrast Media Mol.  
Imaging*, 2011, **6**, 219.
- 92 D. V. Hingorani, E. A. Randtke and M. D. Pagel, *J. Am. Chem. Soc.*,  
2013, **135**, 6396.
- 93 B. Yoo, V. R. Sheth, C. M. Howison, M. J. K. Douglas, C. T. Pineda,  
E. A. Maine, A. F. Baker and M. D. Pagel, *Magn. Reson. Med.*, 2014,  
**71**, 1221.
- 94 V. R. Sheth, G. Liu, Y. Li and M. D. Pagel, *Contrast Media Mol.  
Imaging*, 2012, **7**, 26.
- 95 M. Milne, K. Chicas, A. Li, R. Bartha and R. H. E. Hudson, *Org.  
Biomol. Chem.*, 2012, **10**, 287.
- 96 M. Suchý, A. X. Li, M. Milne, R. Bartha and R. H. E. Hudson,  
*Contrast Media Mol. Imaging*, 2012, **7**, 441.